

# UCLA

## UCLA Previously Published Works

### Title

Activation of specific interneurons improves V1 feature selectivity and visual perception.

### Permalink

<https://escholarship.org/uc/item/0xj2962h>

### Journal

Nature, 488(7411)

### ISSN

0028-0836

### Authors

Lee, Seung-Hee  
Kwan, Alex C  
Zhang, Siyu  
[et al.](#)

### Publication Date

2012-08-01

### DOI

10.1038/nature11312

Peer reviewed



Published in final edited form as:

*Nature*. 2012 August 16; 488(7411): 379–383. doi:10.1038/nature11312.

## Activation of Specific Interneurons Improves V1 Feature Selectivity and Visual Perception

Seung-Hee Lee<sup>1,2</sup>, Alex C. Kwan<sup>1</sup>, Siyu Zhang<sup>1</sup>, Victoria Phoumthippavong<sup>1</sup>, John G. Flannery<sup>1</sup>, Sotiris C. Masmanidis<sup>3</sup>, Hiroki Taniguchi<sup>4</sup>, Z. Josh Huang<sup>4</sup>, Edward S. Boyden<sup>5</sup>, Karl Deisseroth<sup>6</sup>, and Yang Dan<sup>1,2,\*</sup>

<sup>1</sup>Division of Neurobiology, Department of Molecular and Cell Biology, Helen Wills Neuroscience Institute, University of California, Berkeley, California 94720

<sup>2</sup>Howard Hughes Medical Institute, University of California, Berkeley, California 94720

<sup>3</sup>Broad Fellows Program in Brain Circuitry, Kavli Nanoscience Institute, California Institute of Technology, Pasadena, California 91125

<sup>4</sup>Cold Spring Harbor Laboratory, Cold Spring Harbor, New York 11724

<sup>5</sup>Media Laboratory, Biological Engineering, Brain and Cognitive Sciences, and McGovern Institute, Massachusetts Institute of Technology, Cambridge, Massachusetts 02139

<sup>6</sup>Department of Bioengineering, Howard Hughes Medical Institute, Stanford University, Stanford, California 94305

### Abstract

Inhibitory interneurons are essential components of the neural circuits underlying various brain functions. In the neocortex, a large diversity of GABAergic interneurons have been identified based on their morphology, molecular markers, biophysical properties, and innervation pattern<sup>1,2,3</sup>. However, how the activity of each subtype of interneurons contributes to sensory processing remains unclear. Here we show that optogenetic activation of parvalbumin-positive (PV+) interneurons in mouse V1 sharpens neuronal feature selectivity and improves perceptual discrimination. Using multichannel recording with silicon probes<sup>4,5</sup> and channelrhodopsin 2 (ChR2)-mediated optical activation<sup>6</sup>, we found that elevated spiking of PV+ interneurons markedly sharpened orientation tuning and enhanced direction selectivity of nearby neurons.

Users may view, print, copy, download and text and data- mine the content in such documents, for the purposes of academic research, subject always to the full Conditions of use: [http://www.nature.com/authors/editorial\\_policies/license.html#terms](http://www.nature.com/authors/editorial_policies/license.html#terms)

\*To whom correspondence should be addressed. [ydan@berkeley.edu](mailto:ydan@berkeley.edu).

Supplementary Information is linked to the online version of the paper at [www.nature.com/nature](http://www.nature.com/nature).

**Author Information** Reprints and permissions information is available at [www.nature.com/reprints](http://www.nature.com/reprints). The authors declare no competing financial interests. Readers are welcome to comment on the online version of this article at [www.nature.com/nature](http://www.nature.com/nature). Correspondence and requests for materials should be addressed to Y.D. ([ydan@berkeley.edu](mailto:ydan@berkeley.edu)).

**Full Methods** and any associated references are available in the online version of the paper at [www.nature.com/nature](http://www.nature.com/nature).

**Author Contributions** S.H.L. and Y.D. conceived and designed the experiments. S.H.L. performed and organized all the experiments. A.C.K. developed the head-fixed awake mouse preparation and behavioural task setup. S. Z. performed whole-cell recording experiments. V.P. performed some of the virus injection and head plate implant surgeries. J.G.F. supported viral vector preparation. S.C.M. manufactured silicon probe (type II). H.T. and Z.J.H. generated SOM-Cre and VIP-Cre mouse lines. E.S.B. generated Arch-EGFP viral vector. K.D. developed ChR2-EYFP viral vector. S.H.L., A.K., and Y.D. analyzed the data. S.H.L. and Y.D. wrote the manuscript. All authors discussed the results and commented on the manuscript.

These effects were caused by the activation of inhibitory neurons rather than decreased spiking of excitatory neurons, since archaerhodopsin-3 (Arch)-mediated optical silencing<sup>7</sup> of calcium/calmodulin-dependent protein kinase II $\alpha$ -positive (CaMKII $\alpha$ +) excitatory neurons caused no significant change in V1 stimulus selectivity. Moreover, the improved selectivity specifically required PV+ neuron activation, since activating somatostatin (SOM+) or vasointestinal peptide (VIP+) interneurons had no significant effect. Notably, PV+ neuron activation in awake mice caused a significant improvement in their orientation discrimination, mirroring the sharpened V1 orientation tuning. Together, these results provide the first demonstration that visual coding and perception can be improved by elevated spiking of a specific subtype of cortical inhibitory interneurons.

---

To allow specific activation of PV+ interneurons, we injected a Cre-inducible adeno-associated virus (AAV) vector containing the ChR2 gene fused in-frame with the coding sequence for enhanced yellow fluorescence protein (EYFP, Supplementary Fig. 1a)<sup>8</sup> into V1 of a knock-in mouse line expressing Cre-recombinase under the PV promoter (PV-ChR2, see Methods)<sup>9,10</sup>. Three weeks after injection, immunostaining confirmed EYFP expression specific to PV+ neurons (Fig. 1a). To measure the effect of ChR2 activation, we inserted a multichannel silicon probe<sup>4,5</sup> near the injection site for simultaneous recording from all cortical layers (Supplementary Fig. 1b). Upon stimulation with blue (473 nm) laser, a small fraction (12/96, 13%) of the neurons showed significant increases in spontaneous firing rate, while 43% (41/96) showed significant decreases (Fig. 1b, c, Supplementary Fig. 1c). The cells with increased firing exhibited narrower spike waveforms than those with decreased firing (Fig. 1c, inset; peak-trough width,  $0.31\pm 0.12$  vs.  $0.44\pm 0.09$  ms, s.d.), indicating that the PV+ interneurons directly activated by laser were mostly fast-spiking cells<sup>11</sup>. The decreased spiking of other neurons is likely caused by increased inhibition from the activated PV+ neurons.

We then measured orientation tuning and direction selectivity of the neurons using drifting grating stimuli, both with and without ChR2 activation. We found that PV+ neuron activation caused striking changes in the tuning of other neurons. In addition to the overall firing rate decrease, we also observed a marked reduction in orientation tuning width and increase in direction selectivity (Fig. 2a). To quantify these effects, we fitted each tuning curve with a double-Gaussian function (Supplementary Fig. 2a). For all the well-tuned neurons (whose tuning curves with and without ChR2 activation were both well fitted, see Methods), ChR2 activation caused a significant decrease in tuning bandwidth ( $\sigma$ ;  $P < 10^{-4}$ , paired *t*-test; Fig. 2b) and increase in direction selectivity index (DSI;  $P = 0.007$ ; Fig. 2c). However, the preferred orientation ( $\theta_0$ ) remained relatively constant (Fig. 2d). Interestingly, all the putative PV+ neurons (Fig. 1c, white bars) exhibited poor tuning even before laser stimulation, consistent with previous findings<sup>12,13</sup>. Note that while most of the poorly fitted tuning curves showed low signal-to-noise ratio (Supplementary Fig. 2b, c, Examples 1, 2), a few of them had relatively reliable tuning curves exhibiting multiple, irregular peaks (Examples 3–6). Laser stimulation also sharpened the tuning of some of these cells, although the degree of sharpening was not well quantified by curve fitting.

The decrease in  $\sigma$  was correlated with the reduction in firing rate (Supplementary Fig. 3e), suggesting that the enhanced selectivity depends on the increase in inhibition. However, we also wondered whether an overall reduction in cortical firing is sufficient to enhance the selectivity without interneuron activation. As an alternative method to decrease cortical spiking, we expressed the light-activated proton pump Arch<sup>7</sup> in CaMKII $\alpha$ + excitatory neurons by injecting AAV (Supplementary Fig. 1a) into V1 of the CaMKII $\alpha$ -Cre mice<sup>14</sup> (CaMKII $\alpha$ -Arch, Fig. 1d). Arch-mediated partial silencing of CaMKII $\alpha$ + neurons caused decreases in both the spontaneous (Fig. 1e, f, Supplementary Fig. 1c) and visually evoked (Supplementary Fig. 1c, d) firing rates, similar to PV+ neuron activation. However, CaMKII $\alpha$ + neuron silencing caused no significant change in  $\sigma$  ( $P=0.75$ ; Fig. 2f) or DSI ( $P=0.68$ ; Fig. 2g). In addition, there was no significant correlation between the firing rate reduction and change in  $\sigma$  or DSI (Supplementary Fig. 3f, j).

Does the enhanced selectivity require a general increase in inhibition or specific activation of PV+ interneurons? In addition to PV+ neurons, SOM+ and VIP+ neurons constitute two other major subtypes of GABAergic interneurons<sup>2</sup>. To test their roles in shaping V1 selectivity, we induced cell type-specific expression of ChR2-EYFP in SOM-Cre or VIP-Cre mice (Fig. 1g, j). In the SOM-ChR2 mice, laser also caused increased spiking of a few neurons (11/91) and decreased firing of the majority (71/91) (Fig. 1h, i, Supplementary Fig. 1c, d). In fact, compared to the PV-ChR2 group, a higher percentage of neurons showed decreased firing. However, SOM+ activation caused no significant effect on either  $\sigma$  ( $P=0.79$ ; Fig. 2i, j) or DSI ( $P=0.17$ ; Fig. 2i, k). In VIP-ChR2 mice, laser stimulation also induced no significant change in  $\sigma$  ( $P=0.16$ ; Fig. 2m, n) or DSI ( $P=0.16$ ; Fig. 2m, o), and only a mild change in firing rate (Fig. 1k, l, Supplementary Fig. 1c, d). The change in  $\sigma$  showed a negative correlation with firing rate change (Supplementary Fig. 3h), opposite to PV+ activation (Supplementary Fig. 3e). This may be because the VIP+ neurons also innervate inhibitory interneurons<sup>15</sup>, thus causing both inhibition and disinhibition. In addition to  $\sigma$ , tuning measured by orientation selectivity index was also improved by PV+ activation, but not by CaMKII $\alpha$ + silencing or SOM+ or VIP+ activation (Supplementary Fig. 4).

Note that even among the PV-ChR2, SOM-ChR2, and CaMKII $\alpha$ -Arch groups, the degrees of firing rate suppression were not identical. To ensure that the difference in tuning width reduction is not caused by differences in firing rate suppression, we selected neurons from each group that exhibited intermediate levels of suppression (firing rate change  $-0.75$  to  $-0.3$ , Supplementary Fig. 5a). Although the spike rate suppression is well matched across groups within this range (mean rate change:  $-0.51$  (PV),  $-0.50$  (SOM),  $-0.50$  (CaMKII $\alpha$ )), laser stimulation caused a significant decrease in  $\sigma$  in PV ( $-0.19\pm 0.05$ , s.e.m.) but not in SOM ( $0.01\pm 0.09$ ) or CaMKII $\alpha$  ( $-0.05\pm 0.03$ ) group. The magnitudes of reduction in  $\sigma$  were significantly different between the PV and SOM or CaMKII $\alpha$  groups (Supplementary Fig. 5b). We also noticed that neurons in these groups showed different initial tuning widths ( $\sigma_{\text{light-off}}$ ). To ensure that the difference in tuning width reduction was not caused by the difference in  $\sigma_{\text{light-off}}$ , we selected neurons with  $\sigma_{\text{light-off}}$  falling within two ranges: the broad ( $25^\circ$ – $50^\circ$ ) and narrow ( $0^\circ$ – $25^\circ$ ) ranges. Within each range, the median values of  $\sigma_{\text{light-off}}$  were not significantly different across groups, but laser stimulation caused significant

decrease in  $\sigma$  in the PV-ChR2 group (broad:  $-0.28 \pm 0.09$ ; narrow:  $-0.11 \pm 0.05$ ) and not in any other group (Supplementary Fig. 5c, d). Furthermore, within each range the amount of decrease in  $\sigma$  was significantly different between the PV and other groups.

While the lack of effect of VIP+ activation on  $\sigma$  is not surprising given its moderate effect on firing rate, what underlies the difference between SOM+ and PV+ neurons? Tuning of a sensory neuron depends on its FI curve (firing rate vs. input current): subtractive modulation of FI curve causes sharpening of tuning, while divisive modulation has no effect<sup>16</sup>. We thus tested the effects of SOM+ and PV+ activation on neuronal FI functions using *in vivo* whole-cell recording (see Methods). For each neuron we measured firing rate vs. injected depolarizing current. We found that PV+ activation caused a large increase in spiking threshold ( $P=6 \times 10^{-4}$ , paired *t*-test) without significantly changing the slope ( $P=0.34$ , Fig. 3a–d), but SOM+ activation caused a marked reduction of slope ( $P=0.02$ ) without significant change in threshold ( $P=0.18$ , Fig. 3e–h). These effects may be related to the different subcellular targeting of PV+ and SOM+ neurons onto pyramidal neurons (perisomatic vs. dendritic)<sup>17</sup>. When we plotted the median response of each group at each orientation without vs. with laser stimulation, we also found a strong subtractive effect of PV+ activation but primarily divisive effect of SOM+ activation (Supplementary Fig. 6).

Changes in V1 orientation tuning can in principle affect perceptual discrimination<sup>18,19</sup>. To test the functional consequence of sharpened tuning, we applied laser stimulation to awake PV-ChR2 mice while they performed orientation discrimination. The head-restrained mice were trained on a Go/No-Go task and rewarded for licking in response to a grating at one of two orientations<sup>20</sup> (see Methods, Fig. 4a, b, Supplementary Movie 1). For an easy discrimination task (difference between Go and No-Go orientations  $\theta = 90^\circ$ ), the performance measured by the divergence between hit and false alarm rates (Fig. 4c) and discriminability ( $d'$ , Fig. 4d) improved systematically over days. As expected,  $d'$  increased monotonically with  $\theta$  (Fig. 4e). After the performance reached a steady state, we tested the effect of laser and found significant improvement in  $d'$  at a range of  $\theta$  (Fig. 4f, Supplementary Fig. 7a–c). To ensure that the improvement was caused by optical activation of PV+ neurons rather than through the retinal photoreceptors activated by scattered laser, we performed a control experiment in mice that were not virus-infected and found no significant increase in  $d'$  (Fig. 4g). Separate electrophysiological experiments in awake mice showed that PV+ activation also caused a significant sharpening of tuning ( $P < 0.05$ , Supplementary Fig. 8), similar to that in anesthetized mice (Fig. 2a, b). Thus, the sharpening of V1 orientation tuning induced by PV+ activation can facilitate orientation discrimination. Unlike the learning curve shown in Fig. 4d, in which discriminability improved steadily over 5–10 days of training, the effect of PV+ activation showed no systematic change over multiple days of testing (Supplementary Fig. 7d), suggesting that the effect was not caused by learning of a distorted perception due to PV+ activation.

Previous pharmacological experiments have shown that the endogenous level of GABAergic inhibition is necessary for orientation tuning and direction selectivity<sup>21,22</sup>. Our study showed that elevating inhibitory neuron activity above the normal level can further sharpen cortical feature selectivity and improve perceptual discrimination. A recent study showed that PV+ activation only moderately affects the tuning of V1 neurons<sup>23</sup>. This is likely caused by the

relatively low level of PV+ activation compared to our study, as the increase in stimulus selectivity is strongly correlated with the degree of firing rate suppression (Supplementary Fig. 3e,i). Interestingly, studies in awake, behaving primates have shown that increases in task difficulty<sup>24</sup> and attention<sup>25</sup> are accompanied by a preferential increase in the firing of fast-spiking neurons, many of which are likely to be PV+ interneurons<sup>11</sup>. This suggests that the level of inhibitory activity can be dynamically regulated by top-down mechanisms to meet changing behavioral demands.

A long-standing debate on the mechanism for orientation tuning is whether the excitatory and inhibitory inputs exhibit similar tuning<sup>26</sup>. In rodent V1, whether inhibitory interneurons are well tuned has also been controversial<sup>12,13,27</sup>. Our results showed that increase in the untuned activity of inhibitory interneurons is sufficient to sharpen orientation tuning, consistent with previous theoretical prediction<sup>28</sup>. Furthermore, while driving either PV+ or SOM+ interneurons markedly suppressed cortical spiking, only PV+ activation could sharpen orientation tuning. This specificity may be attributable to the powerful perisomatic inhibition exerted by PV+ neurons<sup>1,29</sup>. Recent studies have demonstrated the importance of PV+ neurons in gating developmental plasticity<sup>30</sup> and generating gamma oscillations<sup>9,10</sup>. Our results show that these interneurons also play a unique role in visual coding and perception.

## METHODS SUMMARY

AAV was injected into V1 of adult (P40-60) PV-Cre, CaMKII $\alpha$ -Cre, SOM-Cre, or VIP-Cre mice. For recording and behavioral training in awake mice, head plate was implanted in the same surgery as virus injection; recording or training was performed 2–6 weeks after surgery. For ChR2 (Arch) activation, an optic fiber coupled to blue (yellow/green) laser was placed on top of injection site. For measuring orientation tuning, 8 repeats of drifting sinusoidal grating (spatial frequency, 0.04 cycles/°; temporal frequency, 2 Hz; 100% contrast) were presented in 24 directions (0°–360°) in pseudo-random sequence. Blocks of trials with or without laser were interleaved. To quantify tuning, we fitted each tuning curve by double-Gaussian function. To test orientation discrimination, mice were trained to discriminate between Go and No-Go stimuli (drifting gratings at different orientations) for water reward<sup>20</sup>.

## Methods

### Adeno-associated viral (AAV) vectors

ChR2 fused to the fluorescent protein EYFP (ChR2-EYFP) and Arch fused to EGFP (Arch-EGFP) were cloned into pAAV-MCS (Stratagene) in an antisense direction flanked by a pair of canonical loxP sites and a pair of mutated lox2272 sites. AAV particles (serotype 2) were produced by co-transfection of packaging plasmids into HEK293T cells, and cell lysates were fractionated via iodixanol gradient ultracentrifugation<sup>31</sup>. Viral particles were further purified from the crude fraction by heparin affinity column (HiTrap™ Heparin HP Columns; GE Healthcare), desalted and concentrated with Amicon Ultra Centrifugal Filter (100K, Millipore) ( $1 \times 10^{12} - 10^{14}$  particles ml<sup>-1</sup> in PBS). For ChR2, we used AAV serotype 2/2; for Arch, we used serotypes 2/2 and 2/8. All recombinant viral vectors were cloned in the

genomic DNA backbone of the AAV serotype 2, and we generated the hybrid serotype using different capsids from the corresponding serotypes.

### Virus injection and head plate implant

All experimental procedures were approved by the Animal Care and Use Committee at the University of California, Berkeley. For virus injection, young adult (P40-P60, body weight: 20–30g) PV-Cre (Jackson Laboratory), CaMKII $\alpha$ -Cre (Jackson Laboratory), SOM-Cre (Cold Spring Harbor Laboratory), or VIP-Cre (Cold Spring Harbor Laboratory) mice were anesthetized with ketamine (intraperitoneal, 70 mg per kg of body weight) and supplemented with 1.5% isoflurane and 1.5% O<sub>2</sub>. A craniotomy (~0.5 mm diameter) was made above the monocular region of right V1 (3.7 – 3.8 mm posterior to bregma, 2 mm lateral from midline), and 1  $\mu$ l of AAV (containing > 10<sup>9</sup> viral particles) was injected into the cortex at a depth of 250 – 500  $\mu$ m. For recording and behavioral training in awake mice, custom-designed head plates were implanted right after the virus injection. Small screws (Small Parts) and dental acrylic (Diamond Springs) were used to fix the head plate onto the skull. The skull over the virus injected area was covered by a silicon sealant (Kwik-Cast, WPI).

### Immunohistochemistry

Two weeks after the virus injection, the mice were deeply anesthetized with isoflurane and immediately perfused with chilled 0.1 M PBS followed by 4% paraformaldehyde (wt/vol) in PBS. The brain was removed and post-fixed for 15 h at 4 °C. After fixation, the brain was placed in 30% sucrose (wt/vol) in PBS solution overnight at 4 °C. After embedding and freezing, the brain was sectioned into 40  $\mu$ m coronal slices using a cryostat (Thermo Fisher). Slices were incubated with blocking solution (2% normal goat serum in PBS with 0.5 % Triton-X 100) for 2 h at 20 °C and then with primary antibodies diluted in blocking solution overnight at 4 °C. The following primary antibodies were used: anti-PV primary antibody (PVG-214, Swant; 1:1000), anti-SOM antibody (MAB353, Millipore/Chemicon; 1:200), anti-VIP antibody (20077, ImmunoStar; 1:500), or anti-CaMKII $\alpha$  antibody (sc-13141, Santa Cruz Biotechnology; 1:50). Slices were then washed three times with the blocking solution and incubated with the secondary antibody for 2 h at 20 °C (for PV and VIP, Alexa594-conjugated anti-rabbit IgG, Invitrogen, 1:1000; for CaMKII $\alpha$ , Alexa568-conjugated anti-mouse IgG, Invitrogen, 1:200; for SOM, Cy3-conjugated anti-rat IgG, Jackson ImmunoResearch, 1:200). Slices were washed three times with PBS (10 min each) and mounted with DAPI-containing Vectashield (Vector Laboratories). Fluorescence images were taken under a confocal microscope (Zeiss).

### Electrophysiology

Recording experiments were performed 2–6 weeks after virus injection. For anesthetized experiments, mice were anesthetized with urethane (intraperitoneal, 1.65 g per kg of body weight) supplemented with 1–1.5% isoflurane and restrained in a stereotaxic apparatus (David Kopf Instruments). Body temperature was maintained at 37.5°C via a heating pad (Harvard Apparatus). For recording in awake mice, the body of the mouse was placed in an acrylic tube (2.9 cm inner diameter; McMaster) and the head plate was fixed on a holder attached to the air table. The mouse could move its body inside the tube while the head was

fixed. While the animal was under gas anesthesia (1.5% isoflurane in oxygen), a craniotomy (~1 mm diameter) was made again above the virus injected area and a small portion of the dura was removed to allow insertion of a silicon probe (type I: 27 active channels separated by 50  $\mu\text{m}$ , NeuroNexus Technologies, type II: 16 active channels separated by 35  $\mu\text{m}$ , California Probe<sup>6</sup>). Signals were recorded with the Cheetah 32 channel acquisition system (Neuralynx), filtered at 0.6 – 6 kHz and sampled at 30 kHz. Following the experiment, the mouse was sacrificed with an overdose of isoflurane. The numbers of mice used for electrophysiology experiments were 25 (anesthetized PV-ChR2), 33 (anesthetized CaMKII $\alpha$ -Arch), 25 (anesthetized SOM-ChR2), 9 (anesthetized VIP-ChR2), and 13 (awake PV-ChR2).

Whole-cell recordings were made with an Axopatch 700B amplifier (Axon Instruments). Patch pipettes (3 – 5 M $\Omega$ ) were filled with internal solution containing (in mM) K-gluconate 125, KCl 5, phosphocreatine 10, MgATP 4, GTP 0.4, HEPES 10, and EGTA 1. Data were filtered at 2 kHz, sampled at 10 kHz and digitized by Digidata 1440 (Molecular Devices), and analyzed with custom software in Matlab. Recordings were made under current clamp. Step currents (duration 2 s, amplitude 0 – 1.5 nA) were injected with both laser on and off, each repeated 2 – 4 times. Based on the FI curve (firing rate vs. current amplitude, Supplementary Fig. 6), the current threshold (minimal current to evoke spiking) and the slope were determined by linear regression of the curve from the point of initial spiking.

### Visual stimulation

Visual stimuli were generated with a PC computer containing a NVIDIA GeForce 6600 graphics board and presented with a XENARC 700V LCD monitor (19.7 cm  $\times$  12.1 cm, 960  $\times$  600 pixels, 75 Hz refresh rate, 300 cd m<sup>-2</sup> maximum luminance, gamma corrected with custom software) located 14 cm from the left eye, positioned such that the receptive fields of the recorded neurons were at the center of the monitor. To determine the laminar position of each channel of the silicon probe, contrast-reversal checkerboard stimuli were presented at 2 Hz for 400 times. For measuring orientation tuning and direction selectivity of V1 neurons, full-field drifting gratings (100% contrast, 2 Hz, 0.04 cycles/ $^{\circ}$ , 4 s) were presented at 24 directions (separated by 15 $^{\circ}$ ) in a pseudorandom sequence. After one block of 24 drifting gratings, 4 s of blank stimulus (gray screen) was presented to measure spontaneous firing rate. A total of eight blocks were presented in each experiment. To measure orientation discrimination in the behavioral experiment, drifting gratings of the same contrast and spatiotemporal frequencies (100% contrast, 2 Hz, 0.04 cycles/ $^{\circ}$ , 4 s per trial) were presented to the left eye (see ‘Behavioral Experiment’ below).

### Optical activation and silencing

A blue laser (473 nm) combined with a yellow laser (593 nm) (CrystaLaser) or a green laser (532 nm; Shanghai Laser & Optics Century Co., Ltd.) was connected to an output optic fiber and turned on and off by a stimulator (Grass) under computer control. Optical activation of ChR2 was induced by blue light, and optical silencing by Arch activation was induced by yellow or green light, focused on top of the craniotomy made for virus injection (for behavioral experiment, no new craniotomy was made for optical activation). For each PV-ChR2 or CaMKII $\alpha$ -Arch experiment, the laser power was manually adjusted such that



although the light caused a clear reduction in cortical firing rate, most of the recorded neurons still exhibited visually driven spiking responses (PV-ChR2, 0.5 – 1 mW of blue light, with the majority of experiments at 0.6–0.7 mW; CaMKII $\alpha$ -Arch, 2 – 15 mW of yellow/green light). For SOM-ChR2 and VIP-ChR2 experiments, we used blue light at powers similar to or higher than in the PV-ChR2 experiment (0.6 – 1.5 mW). For VIP-ChR2 experiments increasing the laser power to 2 – 3 mW also did not cause strong suppression of cortical activity. For measuring changes in spontaneous firing rate induced by optical activation or silencing, 30 trials of light stimulation (5 s per trial, 25 s inter-trial interval) were applied while a blank gray screen was presented as the visual stimulus. To measure the effect of optical activation or silencing on visually evoked responses, laser stimulation began 0.5 s before the onset and ended 0.5 s after the termination of each trial of drifting grating stimulation. Since stray laser light could potentially activate the retina (either from the outside or traveling through the cortex), beginning laser stimulation prior to the grating stimuli helped to minimize contamination of the responses to the grating stimuli by transient spiking evoked by the onset of stray laser. We alternated between the blocks of trials (24 orientations per block) with and without laser stimulation. For the whole-cell recording experiments (Supplementary Fig. 6), laser stimulation began 200 ms before the onset of current injection and ended 800 ms after termination of the current step. For the behavioral task, laser stimulation started with the trial and lasted for 5 s, thus covering the entire duration of visual stimulation in each trial (Fig. 4b).

### Data analysis

To determine the laminar position of each recording channel, multiunit activity was aligned to the start time of the flash checkerboard stimuli and averaged across trials. Layers 4 and 6 were identified based on short onset latency of the responses. For single-unit isolation, all channels of the silicon probe were separated into groups (4 channels per group), and spike waveforms were sorted using Klusters (<http://klusters.sourceforge.net>)<sup>32</sup>. To assess the quality of each sorted unit, we computed both Lratio and Isolation Distance<sup>33, 34</sup>. To select high-quality single units, we set the thresholds at Lratio < 0.1 and Isolation Distance > 20 (a unit must satisfy both criteria to be selected), which correspond to < 1% error rate<sup>34</sup>. Among these high-quality single units, only those with firing rates greater than 0.1 spikes/s were included in further analyses. All the analysis was performed in MATLAB (Mathworks).

To quantify orientation tuning and direction selectivity of each neuron, we fitted the firing rate as a function of orientation by the sum of two Gaussian functions with peaks 180° apart:

$$R(\theta) = a_0 + a_1 e^{-\frac{(\theta - \theta_0)^2}{2\sigma^2}} + a_2 e^{-\frac{(\theta - \theta_0 + 180^\circ)^2}{2\sigma^2}}$$

where  $R(\theta)$  is the response at orientation  $\theta$ ,  $a_0$  is the untuned component of the response,  $a_1$  and  $a_2$  are the amplitudes of the two Gaussians,  $\theta_0$  is the preferred orientation, and  $\sigma$  is the standard deviation of the Gaussian function (Supplementary Fig. 2). Tuning width is measured by  $\sigma$ , and direction selectivity (DSI) is measured by:

$$|a_1 - a_2| / (a_1 + a_2)$$

The fitting error was computed as:

$$E = \sum_{\theta} (R_{measure}(\theta) - R_{fit}(\theta))^2 / \sum_{\theta} (R_{measure}(\theta) - \bar{R})^2$$

where  $R_{measure}(\theta)$  and  $R_{fit}(\theta)$  are the measured and fitted responses at  $\theta$ , respectively, and  $\bar{R}$  is the measured response averaged across all orientations. We set a threshold of 0.5 for the fitting error;  $\sigma$  and DSI of a cell were included in the analysis only if the fitting error was below the threshold both with and without laser stimulation.

To quantify the reliability of each measured tuning curve, we computed the signal-to-noise ratio (SNR):

$$SNR = \sum_{\theta} (R(\theta) - \bar{R})^2 / \sum_{\theta} VAR(\theta)$$

Where  $R(\theta)$  is the firing rate at  $\theta$  averaged across all trials,  $\bar{R}$  is the mean firing rate across all orientations, and  $VAR(\theta)$  is the variance of the response at  $\theta$  across trials.

Pearson correlation coefficient ( $r$ ) was used to quantify the relationship between the laser-induced firing rate change and changes in tuning width and direction selectivity.

## Behavioral experiment

Adult PV-ChR2 mice (P60–P100) were water-deprived for 1 day before starting the training. A total of 35 mice were used for the behavioral experiment. During daily training, the mouse was head-fixed and sat in an acrylic tube within a soundproof training box. Tongue licks were detected by a custom-made beam-break lickometer. Training ended when the mouse appeared satiated and stopped licking for several minutes<sup>35</sup>. The entire behavioral experiment consisted of 5 phases: habituation, conditioning, easy discrimination, hard discrimination, and optogenetic experiment.

For habituation (2–3 days), there was no visual stimulus and the mouse was given free water rewards (~4  $\mu$ l) for each lick.

For conditioning (2–3 days), the mouse was trained to lick in response to a visual stimulus (vertically oriented grating drifting rightward; ‘Go stimulus’). Each trial started with a tone (0.1 s duration, 5 kHz), followed by the visual stimulus (starting 1 s after the tone, 4 s in duration), and ended with an inter-trial period of 4 s. If a lick was detected during the last 2 s of the visual stimulation (response window), the mouse was rewarded with ~4  $\mu$ l of water for 2 s (Hit). If no lick was detected during the response window (Miss), water reward was given at the end of the visual stimulus during this conditioning phase. Once the number of Hits exceeded 150 within 30 min, the mouse was advanced to the next phase.

For easy discrimination (5–10 days), each trial had the same temporal structure, but the visual stimulus was either the Go or No-go (horizontally oriented grating drifting upward) stimulus. The Go and No-go trials were randomly interleaved, but the same visual stimulus was never presented more than 3 consecutive times. Licking within the response window of a Go trial (Hit) was rewarded with water, whereas licking in the response window of a No-go trial (false alarm, FA) was punished with a mild air puff (100 ms) and a longer inter-trial interval (8 s, timeout). The mouse was neither rewarded nor punished for Miss (no-lick in a Go trial) or correct rejection (CR, no-lick in a No-go trial). Hit and FA rates were quantified as followings:

$$\begin{aligned} \text{Hit rate} &= \text{number of Hits} / (\text{number of Hits} + \text{number of Misses}) \\ \text{FA rate} &= \text{number of FAs} / (\text{number of FAs} + \text{number of CRs}) \end{aligned}$$

Based on the Hit and FA rates, orientation discriminability ( $d'$ ) was quantified by:

$$d' = \text{norminv}(\text{Hit rate}) - \text{norminv}(\text{FA rate})$$

where norminv is the inverse of the cumulative normal function<sup>21, 36</sup>. Higher  $d'$  values indicate better performance in visual discrimination.

If a threshold performance ( $d' > 1$ ) was reached within 10 days for the easy discrimination task (orientation difference between Go and No-go stimuli,  $\theta = 90^\circ$ ), the mouse was advanced to the next phase. Some of the mice failed to reach the threshold, and they were not further tested.

For hard discrimination (> 5 days), each test block consisted of 20 trials, in which Go and No-go trials at a fixed  $\theta$  were randomly interleaved ( $\theta = 30^\circ, 60^\circ, \text{ or } 90^\circ$ ). To ensure that the mouse stayed motivated, we alternated between a 'relearning' block ( $\theta = 90^\circ$ ) and a 'test' block ( $\theta = 30^\circ, 60^\circ, \text{ or } 90^\circ$ ; the sequence among test blocks of different  $\theta$  was pseudo-random). For each mouse, the orientation of either Go or No-go stimulus was fixed, while  $\theta$  changed across blocks. Discriminability ( $d'$ ) was then measured as a function of  $\theta$ . When  $d' > 0.5$  for  $\theta = 30^\circ$ , we added test blocks with  $\theta = 10^\circ$  (i.e., we alternated between the relearning block with  $\theta = 90^\circ$  and a test block with  $\theta = 10^\circ, 30^\circ, 60^\circ, \text{ or } 90^\circ$ ). The addition of this most difficult block ( $\theta = 10^\circ$ ) often caused a considerable drop of the overall performance, most likely caused by a loss of motivation due to the high failure rate. We continued the training in this phase until the performance recovered to a level comparable to that prior to adding the block with  $\theta = 10^\circ$ .

For the optogenetic experiment, the effect of optical activation of PV+ neurons on orientation discrimination was measured at  $\theta = 10^\circ, 30^\circ, 60^\circ, \text{ and } 90^\circ$ . In each block, laser stimulation was applied in 50% of randomly selected trials, and  $d'$  was analyzed separately for trials with and without laser stimulation. To eliminate the trials near the end of each session, when the mouse was satiated and lost motivation for the task, we only included the trials with > 50% hit rate within 100 consecutive trials. To minimize the amount of laser light reaching the eyes, the optic fiber was shielded by a black tape.

Since very strong suppression of visually driven cortical responses can negatively impact perception, the laser power was chosen carefully to match between the behavioral and electrophysiological experiments. We first measured the loss of laser power through the skull (craniotomy was made for the acute electrophysiological experiments but not for the chronic behavioral experiments) *in vitro* by passing the laser beam through the skull of a mouse previously used in the behavior experiment (note that a small hole was drilled during virus injection several weeks before the behavioral experiment, so the skull at the injection site is thinner than at other places; our calibration was performed at the injection site). We found ~30% loss of power after passing through the skull. Since in the majority of the PV-ChR2 electrophysiology experiments we used 0.6 – 0.7 mW of laser power, which was found to be effective in sharpening the tuning curve without excessive suppression of cortical activity, we chose 0.8 – 1 mW laser power for the behavioral experiments. Each mouse was tested up to 8 sessions (one session per day), and all animals tested with 0.8 – 1 mW laser were included (n = 25).

Among the 25 PV-ChR2 mice tested, 6 were advanced directly from easy discrimination to optogenetic experiment, and the effect of PV activation was tested only at  $\theta = 90^\circ$ ; 10 mice were trained in hard discrimination at  $\theta = 30^\circ, 60^\circ, \text{ and } 90^\circ$ , and the effect of laser was tested at these three angle; the remaining 9 mice were trained in hard discrimination at  $\theta = 10^\circ, 30^\circ, 60^\circ, \text{ and } 90^\circ$  before the effect of laser was tested at all four angles.

## Supplementary Material

Refer to Web version on PubMed Central for supplementary material.

## Acknowledgments

We thank M. Goard, L. Pinto, M. Xu, and M. Viesel for the help with experimental setup, A. Kaluszka for help with data analysis, H. Alitto and M. Poo for discussion and comments on the manuscript. This work was supported by NIH R01 EY018861 and NSF 22250400-42533.

## References

1. Markram H, et al. Interneurons of the neocortical inhibitory system. *Nature Rev Neurosci*. 2004; 5:793–807. [PubMed: 15378039]
2. Xu XM, Roby KD, Callaway EM. Immunochemical characterization of inhibitory mouse cortical neurons: three chemically distinct classes of inhibitory cells. *J Comp Neurol*. 2010; 518:389–404. [PubMed: 19950390]
3. Ascoli GA, et al. Petilla terminology: nomenclature of features of GABAergic interneurons of the cerebral cortex. *Nature Rev Neurosci*. 2008; 9:557–568. [PubMed: 18568015]
4. Blanche TJ, Spacek MA, Hetke JF, Swindale NV. Polytrodes: high-density silicon electrode arrays for large-scale multiunit recording. *J Neurophysiol*. 2005; 93:2987–3000. [PubMed: 15548620]
5. Du JG, et al. High-resolution three-dimensional extracellular recording of neuronal activity with microfabricated electrode arrays. *J Neurophysiol*. 2009; 101:1671–1678. [PubMed: 19091921]
6. Deisseroth K. Optogenetics. *Nature Meth*. 2011; 8:26.
7. Chow BY, et al. High-performance genetically targetable optical neural silencing by light-driven proton pumps. *Nature*. 2010; 463:98. [PubMed: 20054397]
8. Zhang F, et al. Optogenetic interrogation of neural circuits: technology for probing mammalian brain structures. *Nature Protoc*. 2010; 5:439–456. [PubMed: 20203662]

9. Sohal VS, Zhang F, Yizhar O, Deisseroth K. Parvalbumin neurons and gamma rhythms enhance cortical circuit performance. *Nature*. 2009; 459:698–702. [PubMed: 19396159]
10. Cardin JA, et al. Driving fast-spiking cells induces gamma rhythm and controls sensory responses. *Nature*. 2009; 459:663–U63. [PubMed: 19396156]
11. Toledo-Rodriguez M, et al. Correlation maps allow neuronal electrical properties to be predicted from single-cell gene expression profiles in rat neocortex. *Cereb Cortex*. 2004; 14:1310–1327. [PubMed: 15192011]
12. Kerlin AM, Andermann ML, Berezovskii VK, Reid RC. Broadly tuned response properties of diverse inhibitory neuron subtypes in mouse visual cortex. *Neuron*. 2010; 67:858–871. [PubMed: 20826316]
13. Ma WP, et al. Visual representations by cortical somatostatin inhibitory neurons-selective but with weak and delayed responses. *J Neurosci*. 2010; 30:14371–14379. [PubMed: 20980594]
14. Tsien JZ, et al. Subregion- and cell type-restricted gene knockout in mouse brain. *Cell*. 1996; 87:1317–1326. [PubMed: 8980237]
15. David C, Schleicher A, Zusratter W, Staiger JF. The innervation of parvalbumin-containing interneurons by VIP-immunopositive interneurons in the primary somatosensory cortex of the adult rat. *Eur J Neurosci*. 2007; 25:2329–40. [PubMed: 17445231]
16. Ayaz A, Chance FS. Gain modulation of neuronal responses by subtractive and divisive mechanisms of inhibition. *J Neurophysiol*. 2009; 101:958–68. [PubMed: 19073814]
17. Mehaffey WH, Doiron B, Maler L, Turner RW. Deterministic multiplicative gain control with active dendrites. *J Neurosci*. 2005; 25:9968–77. [PubMed: 16251445]
18. Kang KJ, Shapley RM, Sompolinsky H. Information tuning of populations of neurons in primary visual cortex. *J Neurosci*. 2004; 24:3726–3735. [PubMed: 15084652]
19. Schoups A, Vogels R, Qian N, Orban G. Practising orientation identification improves orientation coding in V1 neurons. *Nature*. 2001; 412:549–553. [PubMed: 11484056]
20. Andermann ML, Kerlin AM, Reid RC. Chronic cellular imaging of mouse visual cortex during operant behavior and passive viewing. *Front Cell Neurosci*. 2010; 4
21. Sillito AM. Effectiveness of bicuculline as an antagonist of GABA and visually evoked inhibition in cats striate cortex. *J Physiol-London*. 1975; 250:287–304. [PubMed: 1177143]
22. Nelson S, Toth L, Sheth B, Sur M. Orientation selectivity of cortical neurons during intracellular blockade of inhibition. *Science*. 1994; 265:774–777. [PubMed: 8047882]
23. Atallah BV, Bruns W, Carandini M, Scanziani M. Parvalbumin-expressing interneurons linearly transform cortical responses to visual stimuli. *Neuron*. 2012; 73:159–70. [PubMed: 22243754]
24. Chen Y, et al. Task difficulty modulates the activity of specific neuronal populations in primary visual cortex. *Nat Neurosci*. 2008; 11:974–82. [PubMed: 18604204]
25. Mitchell JF, Sundberg KA, Reynolds JH. Differential attention-dependent response modulation across cell classes in macaque visual area V4. *Neuron*. 2007; 55:131–41. [PubMed: 17610822]
26. Ferster D, Miller KD. Neural mechanisms of orientation selectivity in the visual cortex. *Annu Rev Neurosci*. 2000; 23:441–471. [PubMed: 10845071]
27. Runyan CA, et al. Response features of parvalbumin-expressing interneurons suggest precise roles for subtypes of inhibition in visual cortex. *Neuron*. 2010; 67:847–857. [PubMed: 20826315]
28. Troyer TW, Krukowski AE, Priebe NJ, Miller KD. Contrast-invariant orientation tuning in cat visual cortex: thalamocortical input tuning and correlation-based intracortical connectivity. *J Neurosci*. 1998; 18:5908–5927. [PubMed: 9671678]
29. Di Cristo G, et al. Subcellular domain-restricted GABAergic innervation in primary visual cortex in the absence of sensory and thalamic inputs. *Nature Neurosci*. 2004; 7:1184–1186. [PubMed: 15475951]
30. Hensch TK. Critical period plasticity in local cortical circuits. *Nature Reviews Neuroscience*. 2005; 6:877–888. [PubMed: 16261181]
31. Maheshri N, et al. Directed evolution of adeno-associated virus yields enhanced gene delivery vectors. *Nature Biotech*. 2006; 24:198–204.
32. Hazan L, et al. Klusters, NeuroScope, NDManager: A free software suite for neurophysiological data processing and visualization. *J Neurosci Meth*. 2006; 155:207.

33. Harris KD, et al. Accuracy of tetrode spike separation as determined by simultaneous intracellular and extracellular measurements. *Journal of Neurophysiology*. 2000; 84:401–414. [PubMed: 10899214]
34. Schmitzer-Torbert N, et al. Quantitative measures of cluster quality for use in extracellular recordings. *Neuroscience*. 2005; 131:1–11. [PubMed: 15680687]
35. O'Connor DH, et al. Vibrissa-based object localization in head-fixed mice. *J Neurosci*. 2010; 30:1947–1967. [PubMed: 20130203]
36. Green, D.; Swets, J. *Signal Detection Theory and Psychophysics*. J. Wiley; 1966.

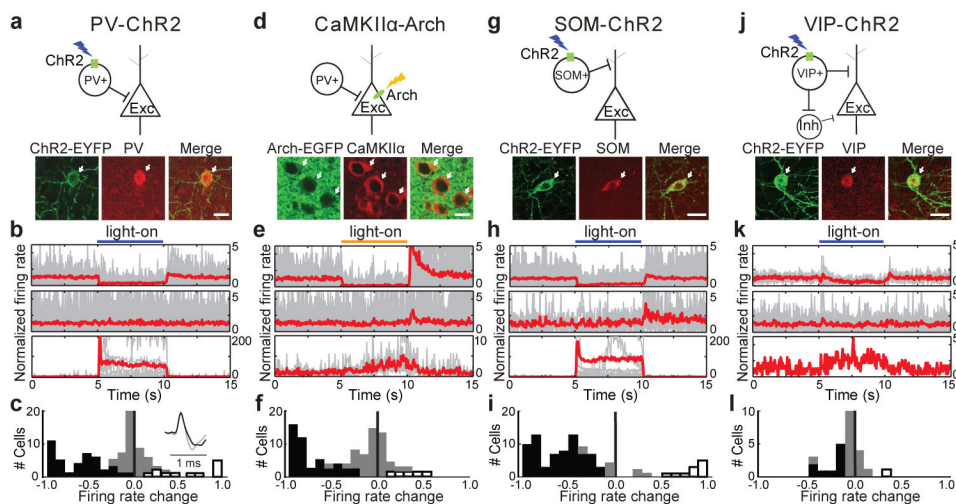


**Figure 1. Optogenetic activation of PV+, SOM+, and VIP+ neurons and silencing of CaMKIIα+ neurons**

**a**, Fluorescence images of immunostained PV+ cells (red) expressing ChR2 EYFP (green). Scale, 20  $\mu\text{m}$ . Top, schematic illustration of experiment in **a–c**. **b**, PSTHs of neurons during 30 repeats of blue laser stimulation. Top, cells showing significant firing rate decrease ( $P < 0.01$ , bootstrap;  $n = 41$ ). Middle, cells without significant change ( $n = 43$ ). Bottom, cells with significant increase ( $n = 12$ ). Gray, individual cells; red, average within each group. Blue bar, duration of laser stimulation (5 s). Firing rate of each cell was normalized by its mean rate over the 5 s before stimulation. **c**, Histogram of firing rate changes. Black, gray, white bars represent cells showing significant decreases ( $P < 0.01$ ), no change, and significant increases, respectively. Inset, spike waveform averaged across cells with significantly decreased (black) or increased (gray) firing; **d–f**, Similar to **a–c**, for Arch-mediated silencing of CaMKIIα+ neurons; **g–i**, for ChR2-mediated activation of SOM+ neurons; **j–l**, for ChR2-mediated activation of VIP+ neurons.

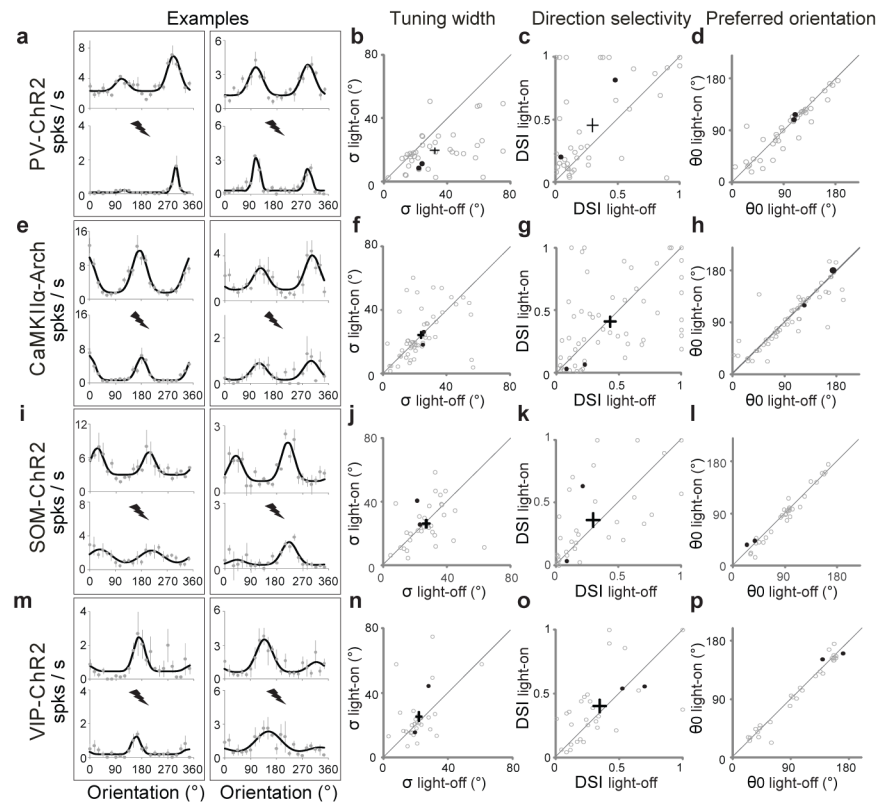


**Figure 2. PV+ activation enhances V1 stimulus selectivity**

**a**, Tuning curves of two cells, each box for one cell. Gray dots, measured firing rates (mean  $\pm$  s.e.m.). Black line, fitted curve. Upper, no laser; lower, laser stimulation (thunderbolt mark). **b–d**, Population summary of ChR2-mediated changes in stimulus selectivity ( $n=41$ ). Each circle represents one cell; cross, population average ( $\pm$ s.e.m.). **b**, Tuning width  $\sigma$ , light-off,  $32.1 \pm 2.9^\circ$  (s.e.m.), light-on,  $19.7 \pm 1.9^\circ$ ; 22% individual neurons showed significant decrease at  $P < 0.01$  (bootstrap), none showed significant increase. **c**, DSI, light-off,  $0.30 \pm 0.05$ , light-on,  $0.45 \pm 0.06$ ; 11% neurons showed significant increase, none showed significant decrease. **d**, Preferred orientation  $\theta_0$ , median difference between light-on and light-off,  $6.2^\circ$ . For neurons in **b–d**, laser reduced visually evoked firing rate from  $5.5 \pm 0.6$  (s.e.m.) to  $2.8 \pm 0.5$  spikes/s ( $P < 10^{-4}$ , paired  $t$ -test). Filled circles, examples cells in **a**. **e–h**, Similar to **a–d**, for CaMKII $\alpha$  silencing. Mean firing rate reduced from  $3.0 \pm 0.4$  to  $2.2 \pm 0.4$  spikes/s ( $n=56$ ,  $P=0.003$ ). **f**,  $\sigma$ , light-off,  $23.6 \pm 1.8^\circ$ , light-on,  $24.3 \pm 2.0^\circ$ , no individual cell showed significant change. **g**, DSI, light-off,  $0.43 \pm 0.04$ , light-on,  $0.41 \pm 0.04$ . **h**,  $\theta_0$ ; median difference,  $5.4^\circ$ . **i–l**, Similar to **a–d**, for SOM-ChR2 mice. Firing rate reduced from  $3.4 \pm 0.6$  to  $1.9 \pm 0.4$  spikes/s ( $P < 10^{-3}$ ). **j**,  $\sigma$ ; light-off,  $26.9 \pm 2.1^\circ$ , light-on,  $26.2 \pm 2.3^\circ$ ,  $n=33$ . No individual cell showed significant change. **k**, DSI; light-off,  $0.29 \pm 0.05$ , light-on,  $0.36 \pm 0.06$ . **l**,  $\theta_0$ ; median difference,  $5.7^\circ$ . **m–p**, for VIP-ChR2 mice ( $n=31$ ). **n**,  $\sigma$ ; light-off,  $21.8 \pm 1.8^\circ$ , light-on,  $25.5 \pm 2.8^\circ$ . **o**, DSI; light-off,  $0.35 \pm 0.05$ , light-on,  $0.41 \pm 0.05$ . **p**,  $\theta_0$ ; median difference,  $5.6^\circ$ .



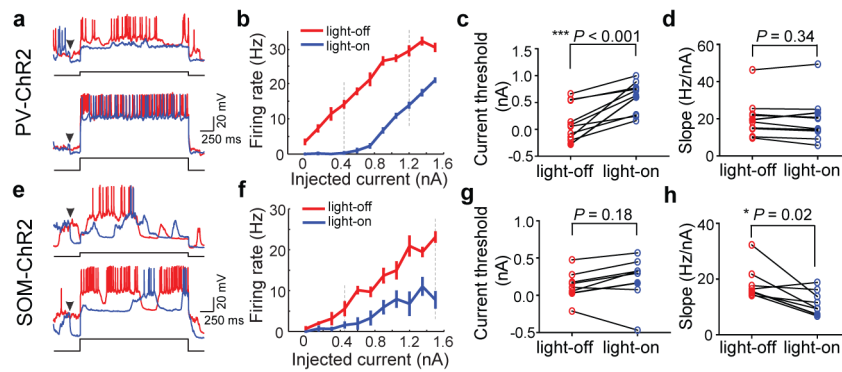


### Figure 3. Effects of PV+ and SOM+ activation on FI function

**a**, Example traces showing neuronal spiking evoked by current injection. Red, voltage trace without laser; blue, with laser. Arrowhead, laser onset (laser offset, 800 ms after current injection, not shown). Current amplitude, 0.45 nA (upper) and 1.2 nA (lower). **b**, FI curve of the cell shown in **a**. Red, without laser; blue, with laser. Error bar,  $\pm$ s.e.m. Dashed lines, current amplitudes shown in **a**. **c**, **d**, Summary of threshold (lowest current that evokes spiking) and FI slope with and without laser. Each symbol represents one cell ( $n=10$ ). **e–h**, Similar to **a–d**, for SOM+ activation ( $n=8$ ).

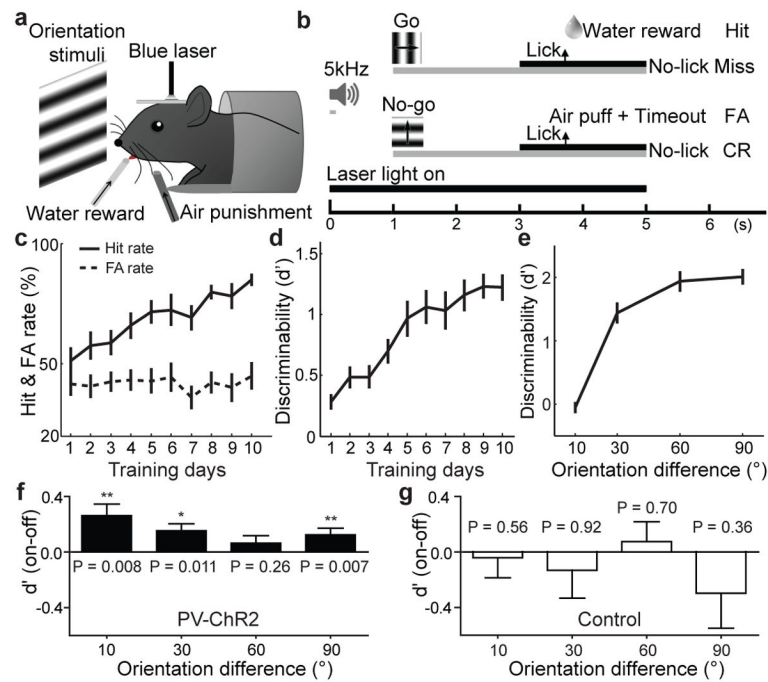


#### Figure 4. PV+ activation improves perceptual discrimination

**a**, Schematic of behavioral experiment. **b**, Task design. Gray bar, duration of visual stimulation. Black bar, response window. FA, false alarm; CR, correct rejection. **c**, Changes in Hit and FA rates of PV-ChR2 mice over training ( $n=25$  mice, mean  $\pm$  s.e.m.). **d**, Changes in  $d'$  over training, **e**,  $d'$  vs.  $\theta$ . Data in **c–e** were collected without laser stimulation. **f**, Laser-induced change in  $d'$  in PV-ChR2 mice, significant at  $\theta = 10^\circ$  ( $P=0.008$ , Wilcoxon signed rank test, 0.032 after Bonferroni correction,  $n = 9$  mice),  $\theta = 30^\circ$  ( $P=0.011$ ,  $n=19$ ), and  $\theta=90^\circ$  ( $P=0.007$ ,  $n=25$ ). **g**, Similar to **f**, for control mice ( $n=10$ ).